International Journal of Nanomedicine

Dovepress
Taylor & Francis Group

Open Access Full Text Article

ORIGINAL RESEARCH

ROS-pH Dual-Responsive Polydopamine Nanoparticles for Targeted Fasudil Delivery Ameliorate Multiple Pathologies in Diabetic Retinopathy

Jiaqi Li[1,*], Zheng Zhong[1,*], Yuhe Tan[1], Xiaohong Ma[1], Ruohong Wang[1], Guoyao Gao[2], Xian Zhang[1], Ziqing Zhou[1], Yin Zhao[1,*], Jia Liu[3], Xufang Sun[4]

[1]Department of Ophthalmology, Tongji Hospital, Tongji Medical College, Huazhong University of Science and Technology, Hubei Key Laboratory of Otolaryngologic and Ophthalmic Diseases, Wuhan, 430068, People's Republic of China; [2]Department of Urology, Tongji Hospital, Tongji Medical College, Huazhong University of Science and Technology, Wuhan, 430030, People's Republic of China; [3]Key Laboratory of Fermentation Engineering (Ministry of Education), National "111" Center for Cellular Regulation and Molecular Pharmaceutics, School of Life and Health Sciences, Hubei University of Technology, Wuhan, 430068, People's Republic of China; [4]Department of Ophthalmology, Tongji Hospital, Tongji Medical College, Huazhong University of Science and Technology, Hubei Key Laboratory of Otolaryngologic and Ophthalmic Diseases, Key Laboratory of Vascular Aging (Ministry of Education), Wuhan, 430068, People's Republic of China

*These authors contributed equally to this work

Correspondence: Xufang Sun; Jia Liu, Email sunxufang2016@163.com; jialiu1207@126.com

Background: The multifaceted pathogenesis of diabetic retinopathy (DR) involves numerous pathways, among which oxidative stress and Rho-associated kinase (ROCK) signaling are critically implicated. The failure of current anti-VEGF monotherapies to address these key pathological processes limits their efficacy. While the ROCK inhibitor Fasudil is a promising candidate, its clinical translation for DR is hindered by poor ocular retention and lack of target specificity.

Methods: We engineered a reactive oxygen species (ROS)- and pH-dual responsive polydopamine nanoplatform (Fasudil@PDA) to deliver Fasudil while concurrently scavenging oxidative stressors.

Results: The Fasudil@PDA nanoparticles achieved a high drug loading capacity of ~28%. The release kinetics were specifically engineered to be responsive to the DR microenvironment. Under high ROS conditions in vitro, the platform demonstrated a sustained and efficient release profile, achieving a cumulative release of 87.3% over 56 days — demonstrating remarkable longevity. Separately, the pH-responsive drug release capability was also confirmed under acidic conditions. The platform effectively neutralized multiple ROS species in vitro and significantly restored endothelial barrier integrity by inhibiting the ROCK/MLC pathway. In a laser-induced choroidal neovascularization model, a single injection suppressed pathological angiogenesis by 45%. In diabetic mice, the same treatment markedly reduced vascular leakage, attenuated neuroinflammation, and restored retinal function, with b-wave amplitudes recovering to near-normal levels.

Conclusion: This study establishes a multi-faceted nanotherapeutic strategy that synergizes sustained, long-acting ROCK inhibition with innate antioxidant activity. Designed to be activated by the pathological cues of DR, including acidic pH and ROS, our approach precisely targets multiple pathological pathways, offering a promising and translatable paradigm for overcoming the limitations of current monotherapies.

Keywords: diabetic retinopathy, ROCK inhibition, reactive oxygen species, pH-responsive, polydopamine nanoparticles, combination therapy

Introduction

Diabetic retinopathy (DR) remains a leading cause of irreversible vision loss worldwide, affecting approximately one-third of the 537 million people living with diabetes globally.[1] This pervasive microvascular complication features

https://doi.org/10.2147/IJN.S584872
Received: 27 November 2025
Accepted: 6 May 2026
Published: 27 May 2026

progressive neurodegeneration and vasculopathy, resulting in blood-retinal barrier (BRB) breakdown, chronic inflammation, and neuronal loss.[2] The current standard care for proliferative DR (PDR) relies on intravitreal anti-vascular endothelial growth factor (anti-VEGF) agents; however, their efficacy remains limited. These biologics primarily target angiogenesis and offer restricted benefits in non-proliferative stages (NPDR), where vascular leakage and inflammation predominate. Moreover, their short intravitreal half-life necessitates frequent injections, increasing treatment burden and risks, while their narrow mechanistic focus fails to address the multifactorial pathogenesis of DR.[3] Hence, there is an urgent clinical need for novel therapies that target upstream drivers, particularly chronic oxidative stress and dysregulated signaling pathways such as Rho-associated protein kinase (ROCK).[4,5] The pathogenesis of DR involves complex metabolic and inflammatory pathways initiated by hyperglycemia. Elevated levels of reactive oxygen species (ROS) and activation of the RhoA/ROCK signaling pathway are critical parallel drivers of disease progression. Both contribute centrally to several pathological processes: (i) BRB disruption via phosphorylation-induced disassembly of tight junction proteins (eg., ZO-1 and occludin); (ii) pathological angiogenesis through both VEGF-dependent and independent mechanisms; and (iii) retinal neurodegeneration mediated by glial activation and neuronal apoptosis.[6,7] Consequently, ROCK inhibition has emerged as a promising therapeutic strategy, demonstrating pleiotropic benefits in preclinical models—including restoration of blood-retinal barrier, suppression of neovascularization, and neuroprotection.[8–12] Fasudil (HA-1077), a clinically approved ROCK inhibitor, represents an attractive candidate for repurposing in DR due to its multi-target effects.[13–17] However, its ocular application is hampered by unfavorable pharmacokinetics, including rapid clearance and poor retinal bioavailability, which necessitate high-frequency dosing and limit therapeutic efficacy.[18–20] These challenges underscore the need for advanced drug delivery systems that enable sustained intraocular release and improved retinal targeting. Nanomedicine offers a promising strategy to overcome these limitations. Innovative nanocarriers can prolong intravitretinal drug residence, reduce administration frequency, and allow for stimulus-responsive release.[21] Among these, polydopamine (PDA) nanoparticles stand out as particularly suitable for DR therapy owing to three key properties: (i) potent intrinsic antioxidant activity capable of scavenging diverse ROS, attributable to their catechol groups; (ii) ROS-responsive biodegradation that enables on-demand drug release at sites of oxidative stress; and (iii) high biocompatibility and favorable retinal safety profiles.[22–25]

Leveraging these advantages, we developed a novel Fasudil-loaded PDA nanoplatform (Fasudil@PDA). This integrated system is designed to synergistically combat DR pathology through three coordinated mechanisms: (1) sustained ROCK inhibition via microenvironment-triggered release of Fasudil; (2) potent reduction of oxidative stress through PDA's ROS-scavenging capacity; and (3) modulation of inflammatory pathways. Our results demonstrate that this nanotherapeutic platform overcomes the limitations of free Fasudil, yielding improved efficacy in DR treatment while maintaining a promising safety profile (Figure 1).

Materials and Methods

Materials

Dopamine hydrochloride, Fasudil, methionine, riboflavin, and nitroblue tetrazolium (NBT) were purchased from Aladdin Biochemical Technology Co., Ltd. (Shanghai, China). Tris-HCl buffer, ethanol (≥ 95%), hydrogen peroxide (30%), and streptozotocin (STZ) were obtained from Sinopharm Chemical Reagent Co., Ltd. (Shanghai, China). The bEnd.3 mouse brain endothelial cell line was purchased from iCell Bioscience Inc. (Shanghai, China; catalog number: TCM40). Dulbecco's Modified Eagle Medium (DMEM) and fetal bovine serum (FBS) were supplied by Gibco (Wuhan, China). Reactive oxygen species (ROS) detection kits (DCFH-DA and DHE), Cell Counting Kit-8 (CCK-8), and fluorescein isothiocyanate-dextran (FITC-dextran) were provided by Beyotime Biotechnology (Shanghai, China). CY5 fluorescent dye was acquired from MedChemExpress (Shanghai, China). Primary antibodies against ROCK1, phosphorylated myosin light chain (p-MLC), zonula occludens-1 (ZO-1), occludin, ionized calcium-binding adapter molecule 1 (Iba-1), RNA-binding protein with multiple splicing (RBPMS), and CD31 were purchased from Cell Signaling Technology (USA). All other reagents were of analytical grade or better, unless otherwise stated.

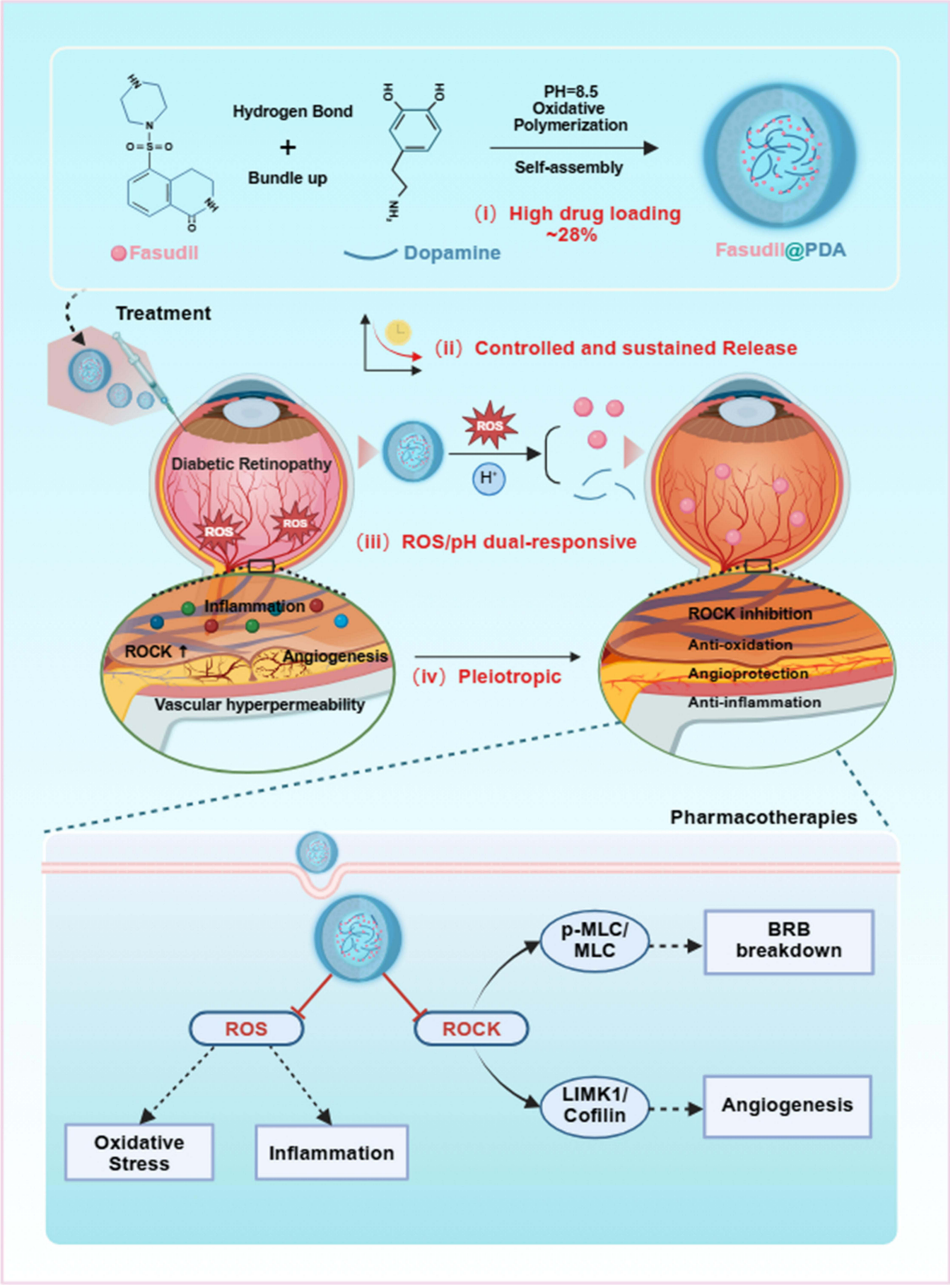

Figure 1 Schematic of the self-assembly and multifaceted therapy of Fasudil@PDA nanoparticles in diabetic retinopathy. Fabricated via pH-triggered polymerization, the nanoparticles exhibit high Fasudil loading and dual-responsive release in the pathological microenvironment. They synergistically alleviate oxidative stress (via PDA's ROS scavenging) and inhibit ROCK signaling (via released Fasudil), thereby targeting key pathologies like vascular leakage, inflammation, and neovascularization. Red —|: Inhibition / Blockade; Solid →: Direct promotion, formation, or activation; ↑: Upregulation.

Preparation of Fasudil@PDA Nanoparticles

Fasudil@PDA nanoparticles were synthesized by oxidative polymerization and self-assembly. Briefly, dopamine hydrochloride (50 mg) and Fasudil (10 mg) were dissolved in 40 mL deionized water under sonication for 15 min. The polymerization was initiated by adding 0.3 mL Tris-HCl buffer (1.5 M, pH 8.8) under continuous stirring at room temperature for 24 h. The nanoparticles were then collected by centrifugation (12,000 rpm, 15 min), washed alternately with deionized water and ethanol (three times each), and lyophilized.

https://doi.org/10.2147/IJN.S584872

Characterization of Fasudil@PDA Nanoparticles

The morphology of the nanoparticles was characterized using scanning electron microscopy (SEM, SU8010, Hitachi, Japan) and transmission electron microscopy (TEM, JEM-2010F, JEOL, Japan), both equipped with energy-dispersive X-ray spectroscopy (EDS) for elemental mapping. Surface chemical composition was analyzed by X-ray photoelectron spectroscopy (ESCALAB 250Xi XPS, Thermo Fisher Scientific, USA). Molecular structure was characterized using Fourier transform infrared spectroscopy (Nicolet iS50 FTIR, Thermo Fisher Scientific, USA). The hydrodynamic diameter and zeta potential were measured with a Zetasizer Nano-ZS instrument (Malvern Panalytical, UK). Drug loading efficiency was determined by sulfur elemental analysis (Vario EL III, Elementar, Langenselbold, Germany) based on the sulfur-to-Fasudil stoichiometry.

ROS Scavenging Capacity Evaluation

The antioxidant activity of Fasudil@PDA nanoparticles was systematically evaluated through three radical scavenging assays. For H_2O_2 scavenging, nanoparticles (0.1–1.6 mg/mL) were incubated with 100 μM H_2O_2 for 30 min, followed by centrifugation and measurement of residual H_2O_2 at 560 nm using a peroxide assay kit. $O_2\cdot^-$ scavenging was assessed in a light-tight chamber, where nanoparticles were incubated with riboflavin (200 μM), methionine (130 mM), and NBT (750 μM) in PBS under white light illumination (20 W, 4000 K, at a distance of 15 cm, yielding an irradiance of approximately 20 mW cm^{-2}), with absorbance measured at 560 nm. DPPH radical scavenging was determined after 20 min incubation with DPPH methanol solution (100 μg/mL), with absorbance read at 517 nm post-centrifugation. All measurements were performed in triplicate using a microplate reader (Infinite F50), with scavenging percentages calculated relative to untreated controls.

ROS-Responsive Release Profile of Fasudil@PDA in vitro

For drug release assessment, Fasudil@PDA nanoparticles (1 mM Fasudil equivalent) were dispersed in PBS (pH 7.4) with or without 100 μM H_2O_2 and incubated at 37 °C. At designated time points (1, 3, 5, 7, 14, 28, and 56 days), 300–500 μL aliquots of supernatant were collected after centrifugation (12,000 g, 10 min) and replaced with equal volumes of fresh buffer to maintain constant release conditions. Released Fasudil was analyzed by LC-MS/MS using:

- HPLC: Dionex Ultimate 3000 with Atlantis T3 column (100×3.0 mm, 3 μm), 0.1% formic acid/acetonitrile gradient (0.4 mL/min)
- MS: Q Exactive with HESI source in positive mode (spray voltage: 3.8 kV; capillary temp: 320°C), full MS/dd-MS^2 (resolution: 70,000/17,500), m/z 50–750.

Cumulative release rate was calculated as (released/total loaded)×100%.

Cellular Uptake Analysis by Fluorescence Microscopy

For fluorescence tracking of nanoparticle internalization, Fasudil@PDA was labeled with Cy5 dye at a 10:1 molar ratio through 1 h incubation at room temperature. bEnd.3 cells were treated with the Cy5-labeled nanoparticles (50 μg/mL Fasudil equivalent) for 4 h at 37 °C under 5% CO_2 atmosphere. After PBS washing, cells were fixed with 4% paraformaldehyde for 15 min at room temperature and counterstained with DAPI. Fluorescence imaging was performed using an Olympus IX83 fluorescence microscope equipped with Cy5 (excitation 640–660 nm/emission 665–740 nm) and DAPI (excitation 340–380 nm/emission 435–485 nm) filter sets. Images were captured using a DP80 dual CCD camera and processed with cell Sens Dimension software.

Intracellular Localization Examination via Transmission Electron Microscopy

For ultrastructural analysis of nanoparticle internalization, bEnd.3 cells were incubated with Fasudil@PDA (100 μg/mL) for 4 h. Cells were then fixed with 2.5% glutaraldehyde in 0.1 M cacodylate buffer (pH 7.4) for 2 h at 4°C, followed by post-fixation with 1% osmium tetroxide. After graded ethanol dehydration (50–100%), samples were embedded in EPON

812 resin and polymerized at 60°C for 48 h. Ultrathin sections (70 nm) were prepared using a Leica UC7 ultramicrotome, double-stained with uranyl acetate (15 min) and lead citrate (5 min), and examined under a JEM-1400Flash TEM (JEOL) operated at 120 kV.

Assessment of Intracellular ROS Generation by Fluorescence Microscopy

bEnd.3 cells were seeded in 12-well plates and grown to 50–60% confluence prior to experimental treatments. Cells were divided into five groups with the following treatments: (1) Control (untreated), (2) 100 μM H_2O_2, (3) H_2O_2 + 30 μM Fasudil, (4) H_2O_2 + 30 μg/mL PDA nanoparticles, and (5) H_2O_2 + 40 μg/mL Fasudil@PDA nanoparticles (equivalent to 30 μM Fasudil). After 24 h incubation, cells were washed with PBS and stained with 500 μL of 10 μM DCFH-DA (diluted 1:1000 in serum-free DMEM) for 30 min at 37 °C. Fluorescence images were acquired using an Olympus IX83 fluorescence microscope equipped with FITC filter set (excitation 465–495 nm/emission 515–555 nm) to detect DCF oxidation.

Quantitative ROS Measurement by Flow Cytometry

For ROS quantification, treated cells were incubated with 10 μM DCFH-DA for 30 min, digested with trypsin, and analyzed by flow cytometry (BD FACSVerse) using FITC channel settings. Data from 10,000 cells/sample were processed using FlowJo software.

Immunofluorescence Staining for Tight Junctions

bEnd.3 cells seeded on coverslips were treated for 24 h under five experimental conditions: control, 100 μM H_2O_2, H_2O_2 + 30 μM Fasudil, H_2O_2 + 30 μg/mL PDA, and H_2O_2 + 40 μg/mL Fasudil@PDA (equivalent to 30 μM Fasudil). Following treatment, cells were fixed with 4% PFA for 15 min, permeabilized with 0.1% Triton X-100 for 10 min, and blocked with 5% BSA for 1 h. Immunostaining was performed using anti-ZO-1 primary antibody (1:200 dilution, 4°C overnight) and Alexa Fluor 594-conjugated secondary antibody (1:500 dilution, 1 h at room temperature), with nuclear counterstaining using DAPI. Fluorescence images were acquired by confocal microscopy using 590/617 nm excitation/emission for ZO-1 and 358/461 nm for DAPI detection.

Western Blot Analysis of Junction Proteins and Signaling Pathways

Cells were divided into five treatment groups: (i) control, (ii) 100 nM advanced glycation end products (AGEs), (iii) AGEs + 30 μM Fasudil, (iv) AGEs + 30 μg/mL PDA, and (v) AGEs + 40 μg/mL Fasudil@PDA (equivalent to 30 μM Fasudil). Following treatment, cells were lysed and proteins were separated by SDS-PAGE, transferred to PVDF membranes, and probed with primary antibodies against ROCK1, phosphorylated myosin light chain (p-MLC), total MLC, ZO-1, occludin, LIM kinase 1 (Limk1), phosphorylated cofilin (p-cofilin), and total cofilin. The relative protein expression levels were quantified using ImageJ software (National Institutes of Health, USA).

In vivo Assessment of Vascular Leakage

Six-to-eight-week-old male C57BL/6 mice were obtained from Hubei Bennt Biological Technology Co., Ltd. (Wuhan, China). All animal procedures were approved by the Institutional Animal Care and Use Committee (No.TJ-C20230301). For the vascular leakage study, mice were randomly divided into five groups (n=6/group): (i) Control (non-diabetic), (ii) DM + PBS, (iii) DM + Fasudil (30 μM), (iv) DM + PDA (30 μg/mL), and (v) DM + Fasudil@PDA (40 μg/mL, equivalent to 30 μM Fasudil). Diabetes was induced by intraperitoneal injection of streptozotocin (STZ, 50 mg/kg/day for 5 consecutive days). Mice with sustained hyperglycemia (blood glucose >16.7 mM for 3 consecutive days) were maintained for 12 weeks.

Intravitreal Injection and FITC-Dextran Extravasation Assay

Following the development of diabetic retinopathy, mice received a single intravitreal injection of their respective treatments. At 1 month after the intravitreal injection, blood-retinal barrier integrity was evaluated. Mice received an intravenous injection of FITC-dextran (50 mg/kg). After 20 minutes of circulation to allow vascular penetration, mice

were euthanized and retinas were isolated for flat-mount preparation. Retinal vasculature was examined by confocal microscopy to assess FITC-dextran extravasation as a measure of vascular leakage.

In vivo Assessment of Pathological Neovascularization

Choroidal neovascularization (CNV) was induced in six-to-eight-week-old male C57BL/6 mice. Following anesthesia with Avertin (300 mg/kg, i.p.) and pupil dilation with 1% tropicamide, laser photocoagulation was performed using a 532 nm laser system (75-μm spot size, 100 ms duration, 200 mW power) to rupture Bruch's membrane. Four treatment groups (n=6/group) were established: (i) CNV + PBS, (ii) CNV + Fasudil (30 μM), (iii) CNV + PDA (30 μg/mL), and (iv) CNV + Fasudil@PDA (40 μg/mL, equivalent to 30 μM Fasudil). A single intravitreal injection of the respective treatment was administered immediately following laser induction.

Immunofluorescence Staining of Retinal Paraffin Sections

Enucleated eyes were fixed in 4% PFA (24 h, 4°C), dehydrated, and paraffin-embedded. Sagittal sections (5 μm) through the optic nerve head were collected on poly-L-lysine-coated slides. After deparaffinization and rehydration, antigen retrieval was conducted using heated citrate buffer (10 mM, pH 6.0). Sections were blocked with 5% normal serum/1% BSA for 1 h and then incubated overnight at 4°C with primary antibodies: anti-IBA1 (1:500) and anti-RBPMS (1:1000). After washing, sections were incubated with fluorescent secondary antibodies (1 h, room temperature, dark). Nuclei were stained with DAPI, and slides were mounted with anti-fade medium for fluorescence microscopy analysis.

In vivo ROS Scavenging Assessment by DHE Staining

Paraffin-embedded sections were dewaxed, rehydrated, and subjected to antigen retrieval following standard protocols. After PBS washing (3×1 min), sections were incubated with 10 μM DHE in a light-protected humidified chamber at 37 °C for 30 min. Following additional PBS washes, slides were mounted with antifade medium and imaged by fluorescence microscopy (excitation/emission: 518/605 nm) to evaluate ROS generation.

Flash Electroretinography (fERG) Recording

After 12-hour dark adaptation, mice were anesthetized with Avertin (300 mg/kg, i.p.) and pupils were dilated with 1% tropicamide. Electrodes were positioned as follows: reference (forehead), ground (tail), and active (corneal contact). Following corneal hydration with saline, fERG responses were recorded under scotopic conditions using single-flash stimuli (2.7 cd·s/m²) to simultaneously elicit rod and mixed rod/cone responses. Signal acquisition was performed with bandpass filtering (0.3–300 Hz) at 1 kHz sampling rate.

Statistical Analysis

Data are presented as mean ± standard deviation (SD). Statistical analyses were performed using GraphPad Prism 9 (GraphPad Software, San Diego, CA, USA). The normality of data distribution was confirmed using the Shapiro–Wilk test, and homogeneity of variances was verified with Brown-Forsythe test. For comparisons among multiple groups, one-way analysis of variance (ANOVA) was performed, followed by Tukey's post hoc test for multiple comparisons. The drug release profile was analyzed using repeated measures ANOVA. A value of $p < 0.05$ was considered statistically significant. The value of n represents the number of biologically independent samples or animals per group.

Results and Discussion

Bioinformatic Identification and Experimental Validation of ROCK Pathway Activation in Diabetic Retinopathy

To identify novel signaling pathways involved in DR, we analyzed the publicly available transcriptomic dataset GSE94019, which includes data from human proliferative diabetic retinopathy (PDR) fibrovascular membranes—pathological tissues rich in activated endothelial cells—and normal retinal endothelial samples.

KEGG pathway analysis indicated significant enrichment in pathways related to regulation of the actin cytoskeleton ($P = 3.2\times10^{-4}$), within which the RHO/ROCK signaling pathway emerged as a central player. Reactome analysis also identified RHO/ROCK among the most significantly altered pathways ($P = 1.8\times10^{-5}$; Figure 2a and b). Consistently, we observed pronounced upregulation of RHOA ($P = 0.007$) and its key effector ROCK1 ($P = 0.016$; Figure 2c), suggesting potential involvement of this pathway in DR pathogenesis.

To ascertain the cell-type specificity of RHO/ROCK activation, we reanalyzed a single-cell RNA-seq dataset from murine retinas, focusing on retinal endothelial cells—a major cell type affected in DR (GSE243100; Figure 2d). Diabetic endothelial cells exhibited substantially elevated expression of both RHOA ($P < 2.0\times10^{-16}$) and ROCK1 ($P = 7.9\times10^{-13}$) compared to non-diabetic controls (Figure 2e). Furthermore, the expression of RHOA and ROCK1, which was only weakly correlated in controls ($r = 0.64$, $P = 0.36$), became strongly correlated in diabetic retinas ($r = 0.86$, $P = 0.003$; Figure 2f), suggesting a disease-associated synergistic upregulation.

Moreover, unbiased pathway analysis connected RHO/ROCK activation to leukocyte transendothelial migration, actin cytoskeleton reorganization, focal adhesion, and vascular smooth muscle contraction (Figure S1). Gene Set Enrichment Analysis (GSEA) further revealed significant enrichment of gene sets related to "regulation of angiogenesis" (GO:0045765) and "endothelial cell migration" (GO:0043542), with leading-edge genes ranking among the top 20% of diabetes-upregulated transcripts (Figures S2 and S3). These findings implicate RHO/ROCK in a pathogenic network coordinating cytoskeletal dynamics, barrier dysfunction, and angiogenic signaling.

Given the established role of RHO/ROCK in regulating endothelial contractility, permeability, and leukocyte adhesion—hallmarks of DR—we next experimentally validated these predictions. In streptozotocin-induced diabetic mice, immunofluorescence imaging revealed pronounced vessel-specific upregulation of ROCK1 (Figure 2g). Western blot analysis further confirmed a 2.3-fold increase in ROCK1 protein expression in diabetic retinas ($P < 0.01$; Figure 2h and i), solidifying the disease-relevant activation of this pathway.

Thus, by integrating bioinformatic discovery with experimental validation, we demonstrate that diabetic retinopathy is characterized by robust activation of the RHO/ROCK pathway within retinal endothelial cells, which drives a genetic program underlying microvascular dysfunction and pathological angiogenesis.

Synthesis and Characterization of Fasudil-Loaded Polydopamine Nanoparticles

Having established the activation of the ROCK pathway in diabetic retinopathy (Figure 2), we selected the clinically approved ROCK inhibitor Fasudil for repurposing, based on its established safety profile and documented vascular protective effects. However, the therapeutic efficacy of Fasudil is limited by both the multifactorial pathology of diabetic retinopathy and its own pharmacological drawbacks, including poor ocular pharmacokinetics and lack of retinal targeting. To address these challenges, we developed Fasudil@PDA nanoparticles that co-deliver Fasudil and the antioxidant polydopamine, thereby simultaneously targeting pathological signaling and oxidative stress.

Synthesis and Structural Confirmation

Fasudil@PDA nanoparticles were synthesized using a facile one-pot method (Figure 3a). Dopamine hydrochloride and Fasudil were first dissolved in an acidic aqueous solution. Upon raising the pH to ~8.5 with Tris-base, Fasudil precipitated to form nucleation cores while dopamine oxidized and polymerized, resulting in the formation of core–shell nanoparticles with a Fasudil-rich core and a polydopamine shell.TEM and SEM imaging revealed spherical, monodisperse nanoparticles (Figures 3b and S4). Elemental mapping showed uniform distribution of carbon, nitrogen, oxygen, and sulfur (Figures 3c and S5); the distinct sulfur signal served as supporting evidence for Fasudil incorporation, further corroborated by FTIR and XPS analyses. FTIR spectra provided additional evidence for successful loading, with the appearance of characteristic Fasudil sulfonyl vibrations at 1350 cm^{-1} and 1150 cm^{-1} (Figure 3d). The XPS survey spectrum (Figure 3e) was consistent with these findings, showing a clear S2p peak and enhanced N1s intensity, further supporting the presence of Fasudil within the nanoparticles.

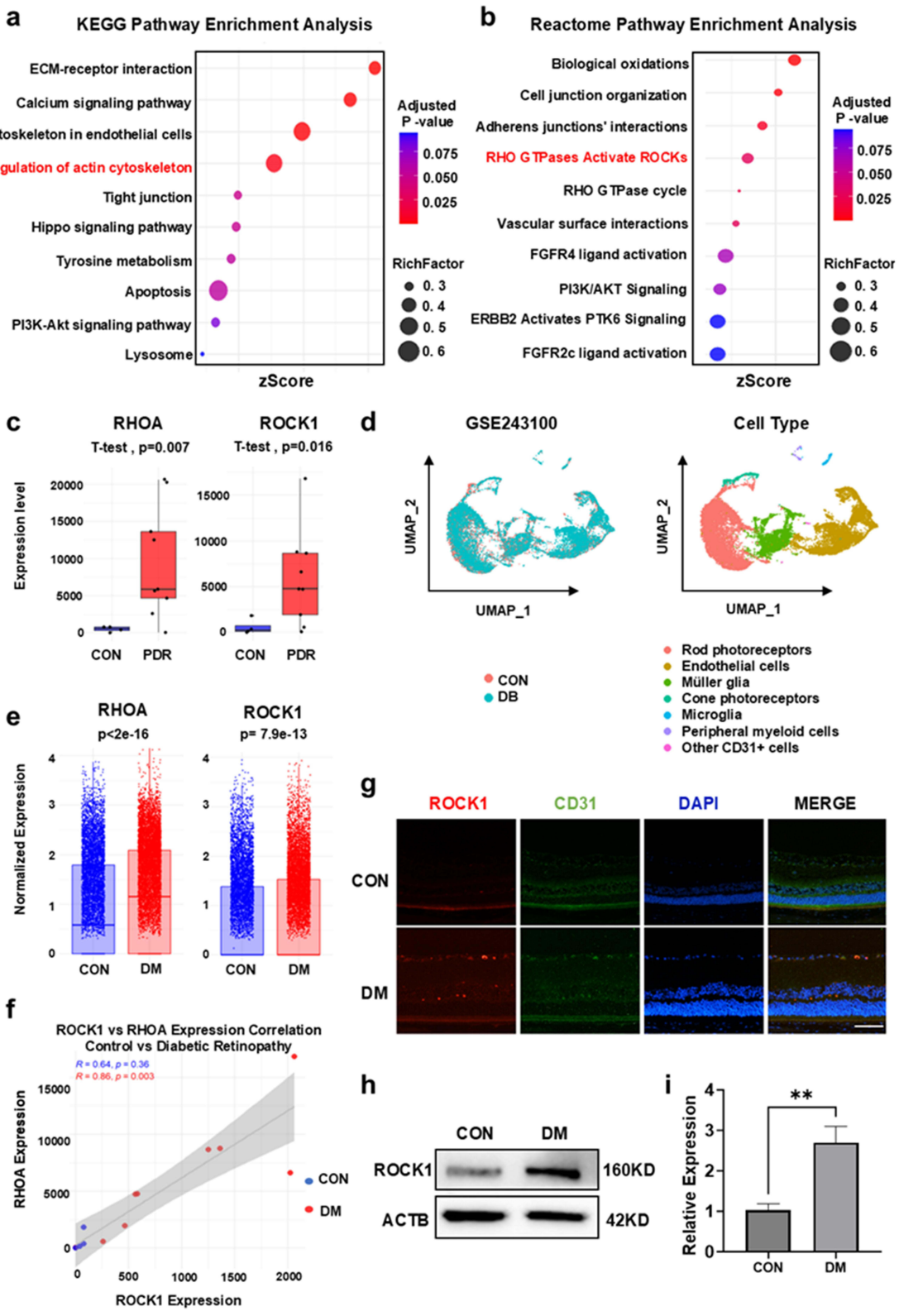

Figure 2 Integrated Bioinformatic and Experimental Analysis Implicates ROCK Signaling in Diabetic Retinopathy Pathogenesis. (**a**) KEGG enrichment analysis of endothelial cells isolated from human proliferative diabetic retinopathy (PDR) fibrovascular membranes (GSE94019). (**b**) Reactome pathway enrichment analysis of differentially expressed genes from human PDR samples. (**c**) Differential gene expression of *RHOA* and *ROCK1* in human PDR versus control samples. (**d**) Uniform Manifold Approximation and Projection (UMAP) visualization of mouse CD31$^+$ cells from single-cell RNA sequencing data (GSE243100). (**e**) Expression analysis of *RHOA* and *ROCK1* in mouse retinal samples from control and diabetic mellitus (DM) groups. (**f**) Correlation analysis between *RHOA* and *ROCK1* expression in mouse retinal samples. (**g**) Fluorescence microscopy images showing ROCK1 expression in mouse retina. Scale bar = 100 μm. (**h**) Western blot analysis of ROCK1 protein expression in mouse retina samples. (**i**) Quantitative analysis of ROCK1 protein expression levels normalized to β-actin. Data are presented as mean ± SD; **p < 0.01.

https://doi.org/10.2147/IJN.S584872

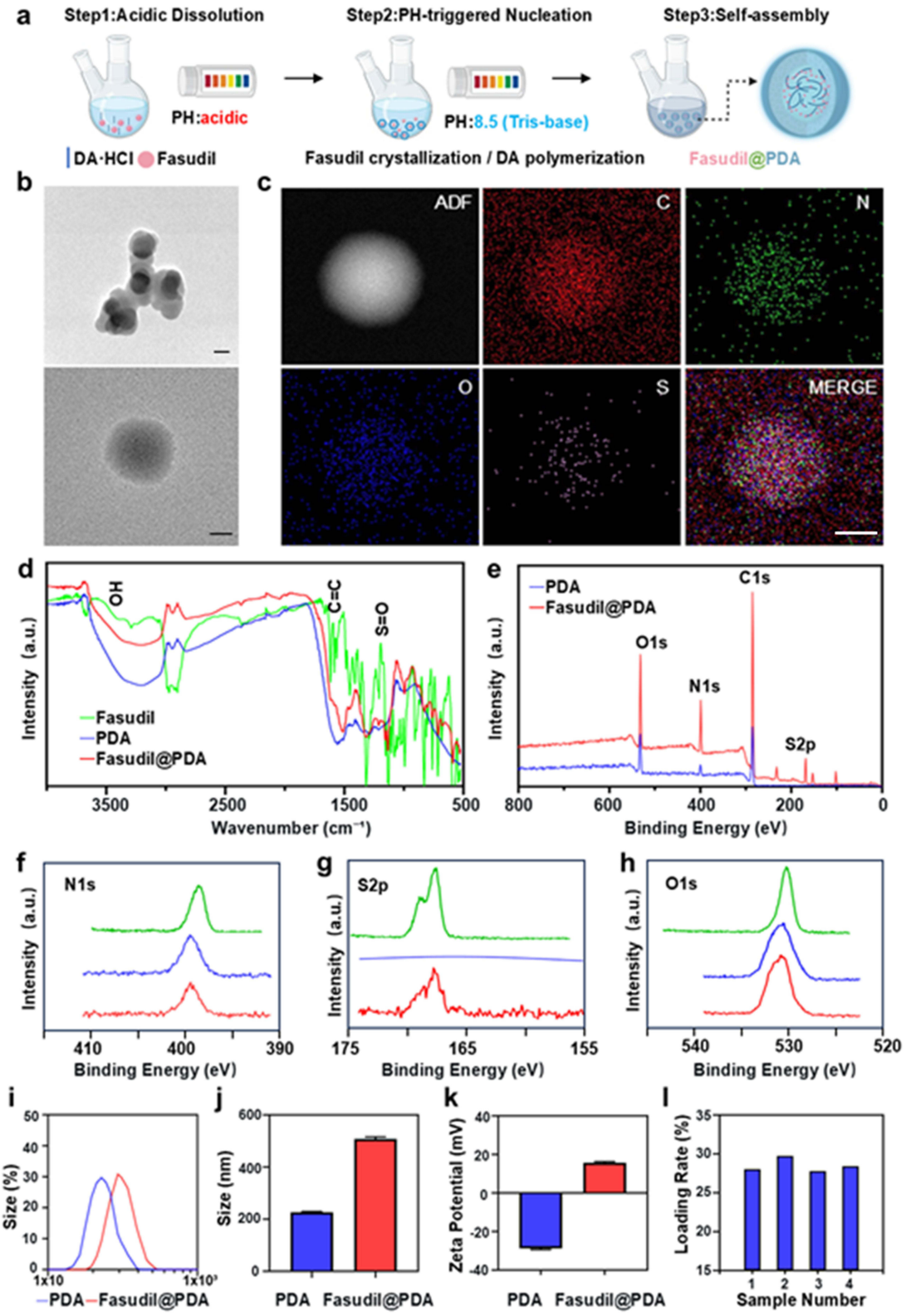

Figure 3 Preparation and characterization of Fasudil@PDA nanoparticles. (**a**) Schematic of the one-pot synthesis process for Fasudil@PDA NPs, including acidic dissolution, pH-triggered nucleation, and co-polymerization/self-assembly. (**b**) TEM image of the as-synthesized Fasudil@PDA NPs. Scale bar, 200 nm. (**c**) Elemental mapping C, N, O, S of a single Fasudil@PDA NP, showing uniform distribution of S and confirming successful Fasudil incorporation. Scale bar, 100 nm. (**d**) FTIR spectra of pure PDA and Fasudil@PDA NPs. (**e**) XPS survey spectrum and (**f–h**) high-resolution N1s, S2p, and O1s spectra of Fasudil@PDA NPs, with observed binding energy shifts suggesting hydrogen bonding between Fasudil and PDA. (**i** and **j**) Hydrodynamic size distributions of PDA and Fasudil@PDA NPs. (**k**) Zeta potentials of PDA and Fasudil@PDA NPs. (**l**) Drug loading capacity of Fasudil@PDA NPs across different batches.

https://doi.org/10.2147/IJN.S584872

Hydrogen Bonding Mediates Assembly and Stability

Directional non-covalent interactions played a critical role in nanoparticle assembly. FTIR spectroscopy provided the initial evidence for such interactions: the broad O–H/N–H stretching band at ~3400 cm^{-1} exhibited noticeable broadening and a redshift (Figure 3d), which is a classic spectroscopic signature of hydrogen bonding, suggesting the possibility of strong intermolecular interactions between Fasudil and PDA.

High-resolution XPS spectra then offered definitive evidence to pinpoint the exact nature and directionality of these bonds. The N1s spectrum (Figure 3f) showed a positive binding energy shift and broadening of the amine/imine peak, indicating reduced electron density at nitrogen sites and identifying N–H groups from PDA as hydrogen bond donors. Complementarily, the S2p spectrum (Figure 3g) exhibited a positive binding energy shift of the sulfonyl group, confirming decreased electron density at oxygen atoms and their role as hydrogen bond acceptors from Fasudil. Further supporting evidence came from the C1s spectrum (Figure S6), which revealed binding energy shifts and altered line shapes consistent with the proposed intermolecular hydrogen bonding. These reciprocal changes, supported by alterations in the O1s spectrum (Figure 3h), demonstrate that N–H...O=S hydrogen bonding is the key interaction governing nanoparticle self-assembly and stability.

Together, FTIR and XPS analyses formed a coherent and robust evidence chain, from the initial suggestion of hydrogen bonding to its precise elemental confirmation. It conclusively establishes that hydrogen bonding is the primary driving force behind the co-assembly process.

This robust hydrogen-bonding network enhances nanoparticle integrity, preventing drug leakage. Moreover, as hydrogen bonds are pH-responsive, the mildly acidic retinal environment in diabetic retinopathy (pH ≈6.8–7.2) may promote targeted drug release, highlighting the therapeutic relevance of this mechanism.[26,27]

Physicochemical Properties and Loading Efficiency

The Fasudil@PDA nanoparticles exhibited a hydrodynamic diameter of 497.8 ± 23.5 nm (Figure 3i and j), significantly larger than pure PDA nanoparticles (224.5 ± 12.1 nm, $p < 0.01$), consistent with successful drug encapsulation. Zeta potential measurements showed a positive surface charge of +14.4 ± 2.1 mV (Figure 3k), which may facilitate cellular uptake through electrostatic interactions with negatively charged cell membranes.[28,29] The drug loading capacity, determined by quantifying the characteristic sulfur element of Fasudil, reached approximately 28% (Figure 3l). This value represents a ~70-fold improvement over reported Fasudil loadings in PLGA systems (typically ~0.4%),[30] a fundamental advantage directly attributed to the inherent molecular compatibility between Fasudil and PDA that enables efficient co-assembly, rather than passive physical encapsulation.

In summary, we have successfully developed and characterized Fasudil@PDA nanoparticles using a scalable one-pot synthesis approach. Multiple lines of evidence confirm that hydrogen bonding is the dominant force behind nanoparticle assembly, endowing the system with both structural stability and microenvironment-responsive release potential. These properties make Fasudil@PDA a promising platform for targeted therapy in diabetic retinopathy.

Dual-Responsive Fasudil@PDA Nanoparticles Enable Synergistic Therapy for Diabetic Retinopathy Through ROS Scavenging and pH-Enhanced Drug Release

Reactive oxygen species (ROS)—including superoxide anion (O_2^-), hydrogen peroxide (H_2O_2), hydroxyl radical (•OH), and peroxyl radicals (ROO•)—play a critical role in the pathogenesis of diabetic retinopathy by inducing oxidative damage and inflammatory responses.[31,32] Owing to its catechol groups, polydopamine (PDA) possesses notable antioxidant properties, making it an effective ROS-scavenging platform. We confirmed that Fasudil@PDA maintains antioxidant performance comparable to unmodified PDA at physiologically relevant concentrations. Through standardized assays, the conjugate effectively neutralized H_2O_2, O_2^-, and DPPH radicals (Figure 4a–c), confirming that the antioxidant functionality was preserved after Fasudil incorporation.

ROS-triggered degradation of Fasudil@PDA was visually apparent from its concentration-dependent color shift from dark brown to light yellow upon H_2O_2 treatment (Figure 4d), indicating oxidative breakdown of the PDA structure. This was further substantiated by UV-Vis spectroscopy, which showed a progressive decline in absorbance with increasing H_2O_2 concentration (Figure 4e).

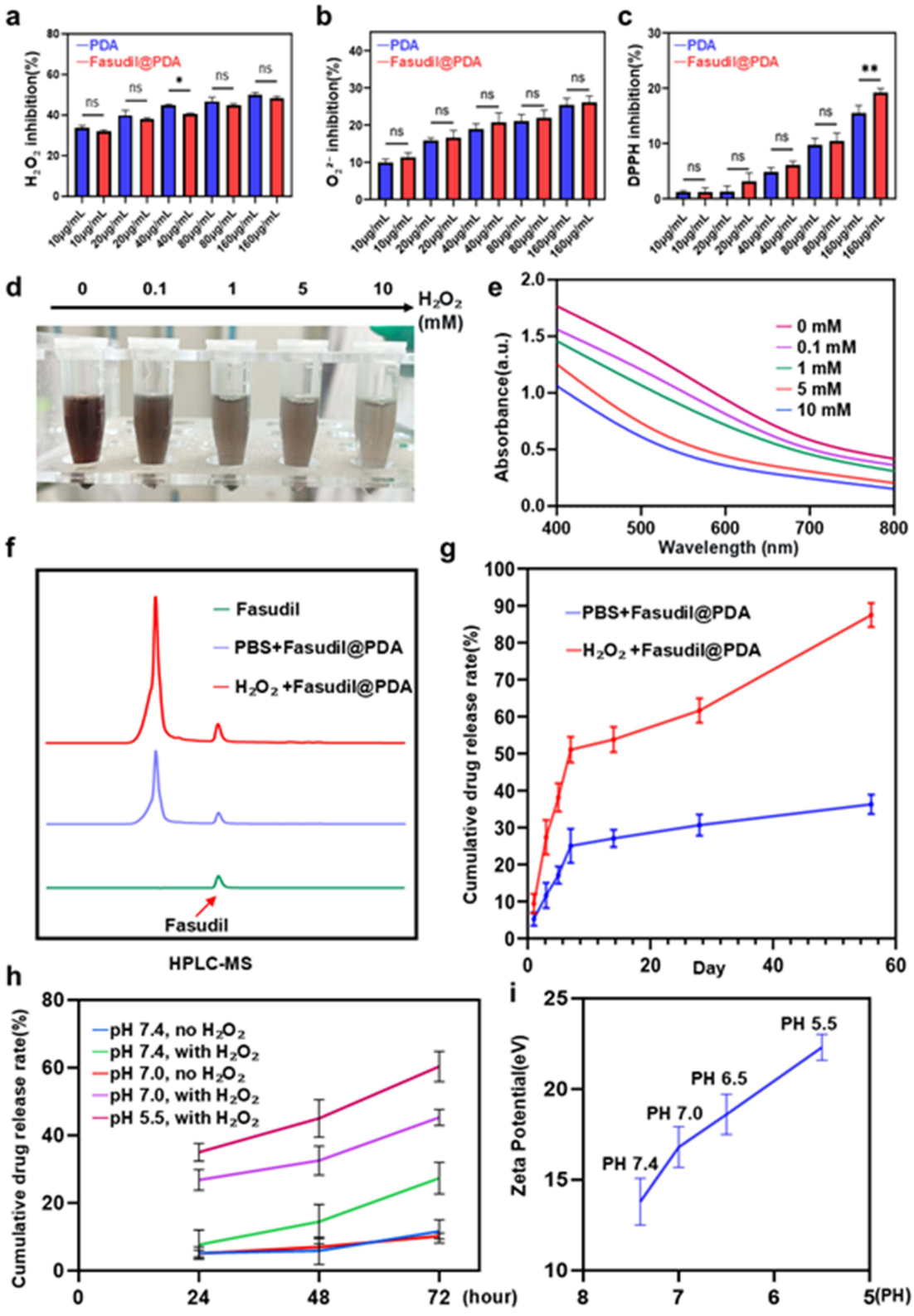

Figure 4 Comprehensive evaluation of the antioxidative, degradation, and stimuli-responsive drug release properties of Fasudil@PDA nanoparticles. (**a**–**c**) Concentration-dependent in vitro antioxidant capacity of Fasudil@PDA and PDA, as assessed by scavenging of (**a**) H_2O_2, (**b**) superoxide anion, and (**c**) DPPH radicals. Data are presented as mean ± SD (n = 3). Statistical significance is indicated as *p < 0.05, **p < 0.01; ns denotes no significant difference (p ≥ 0.05). (**d**) Representative digital images of Fasudil@PDA NPs after incubation with varying concentrations of H_2O_2 for 72 h. (**e**) UV-Vis spectra of the nanoparticles following H_2O_2-induced degradation. (**f**) HPLC quantification of Fasudil release from Fasudil@PDA NPs in PBS without and with 100 μM H_2O_2. (**g**) Long-term cumulative release profile of Fasudil over 56 days in PBS at 37 °C. (**h**) In vitro drug release profiles of Fasudil@PDA NPs under various pH (7.4, 7.0, 5.5) and ROS conditions. (**i**) Zeta potential of Fasudil@PDA NPs measured at varying pH values.

https://doi.org/10.2147/IJN.S584872

HPLC-MS analysis of the release medium under oxidative conditions confirmed the structural integrity of released Fasudil, showing a molecular ion peak (m/z = 292.11147) consistent with the standard compound (Figure S7). Release kinetics demonstrated strong ROS-dependent behavior, with significantly accelerated Fasudil release under 100 μM H_2O_2 compared to the PBS control (Figure 4f). The cumulative release profile (Figure 4g) demonstrated sustained release properties appropriate for diabetic retinopathy treatment, showing a 3-fold increase after 7 days under high ROS conditions without initial burst release (<15% at 24 h). Remarkably, the system steadily released over 56 days, reaching a cumulative total of 87.3 ± 4.1%, highlighting its exceptional sustainability.

TEM images of degradation products (Figure S8) revealed that nanoparticles maintained spherical morphology despite particle size reduction (~100 nm after 28 days). Elemental mapping (Figure S9) confirmed homogeneous Fasudil distribution (via S-signal), consistent with a surface-eroding disintegration mechanism that supports both ROS scavenging and prolonged drug release—an essential feature for managing chronic oxidative stress in diabetic retinopathy.

Given the presence of hydrogen bonding between Fasudil and PDA, we further explored the pH-responsive release properties of the nanoparticles. Notably, Fasudil@PDA exhibited significantly enhanced drug release under acidic conditions (from pH 7.4 down to 6.5), particularly in the presence of ROS stimulation. A remarkable synergistic release effect was observed at mildly acidic pH (7.0), where the combined stimuli of acidity and oxidative conditions resulted in release kinetics surpassing those induced by either stimulus alone (Figure 4h).

This accelerated release is mechanistically attributed to two interrelated factors: first, the protonation of functional groups under acidic conditions weakens the N–H···O=S hydrogen bonds between Fasudil and PDA—as directly evidenced by XPS and FTIR analyses; second, acidification induces a substantial increase in the surface positive charge of the nanoparticles, with the zeta potential rising from approximately +8 mV at physiological pH (7.4) to +25 mV under acidic conditions (pH 5.5) (Figure 4i). The resulting enhancement in electrostatic repulsion between protonated drug molecules and the carrier matrix further promotes efficient and responsive drug release. This pH-sensitized release mechanism constitutes a key innovation of our system: the ability to exploit the mildly acidic microenvironment typical of pathological sites such as diabetic retinopathy, thereby enabling targeted and condition-triggered drug liberation with improved spatial and temporal control.

Overall, this study establishes a dual-responsive nanoparticle system that efficiently reacts to both ROS and acidic pH —hallmarks of the diabetic retinopathy microenvironment. We have thoroughly verified the ROS-responsive degradation and release behavior of Fasudil@PDA, confirming the retention of PDA's antioxidant function and the structural integrity of released Fasudil. Importantly, compared to previously reported Fasudil delivery systems (eg., PLGA microspheres with ~40% release over 28 days[30]), our Fasudil@PDA achieves a superior 87% cumulative release over 56 days under ROS stimulus, highlighting the advantage of hydrogen-bonding-mediated co-assembly. Furthermore, while other combination nanotherapies for DR often require separate drug encapsulation, our single-platform approach integrates both ROCK inhibition and ROS scavenging, offering manufacturing simplicity and enhanced clinical translatability. This nanoplatform thus enables context-dependent drug release precisely tailored to the pathological cues of diabetic retinopathy.

Cellular Internalization and ROS Scavenging by Fasudil@PDA Nanoparticles

To achieve therapeutic efficacy, Fasudil@PDA nanoparticles must be efficiently internalized.[33,34] We found that Fasudil@PDA nanoparticles are effectively internalized by vascular endothelial cells and exhibit potent reactive oxygen species (ROS)-scavenging activity. To visualize cellular uptake, Fasudil@PDA was conjugated with CY5, a far-red fluorescent dye (ex/em: 650/670 nm). Free CY5, due to its poor membrane permeability, showed negligible cellular entry, whereas fluorescence microscopy revealed pronounced perinuclear accumulation of Fasudil@PDA-CY5 in bEnd.3 endothelial cells (Figure 5a and b). Transmission electron microscopy (TEM) further confirmed that internalization occurs via endocytosis (Figure 5c), with subsequent trafficking to lysosomes. Notably, within these acidic compartments, the nanoparticles undergo enzymatic degradation leading to maximal drug release (Figure 5d, arrow), underscoring the stimuli-responsive precision of this delivery system.

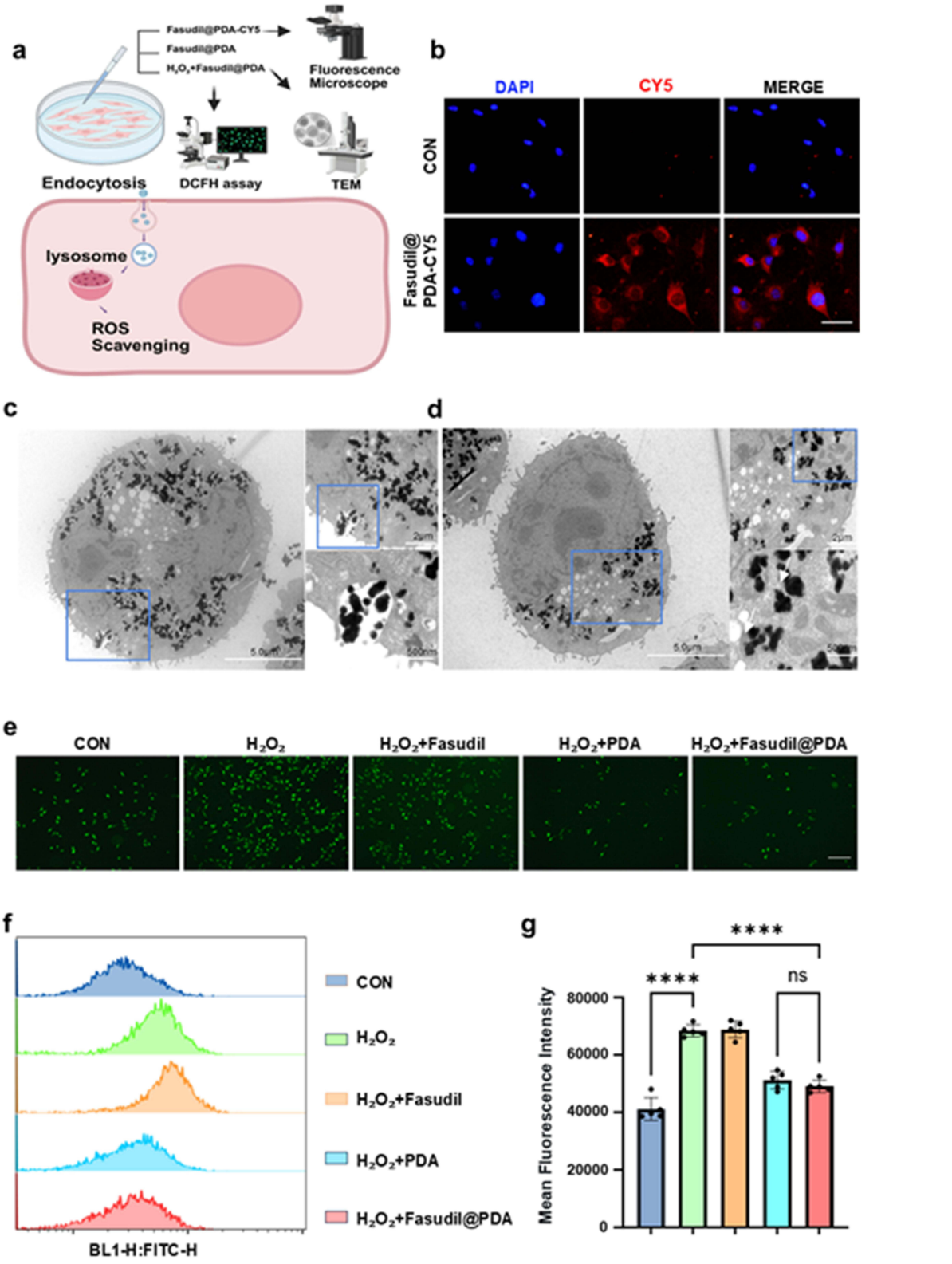

Figure 5 Cellular uptake and antioxidant effects of Fasudil@PDA nanoparticles. (**a**) Schematic of experimental design. (**b**) Cellular uptake of CY5-labeled Fasudil@PDA. Fluorescence microscopy images (DAPI: nucleus; CY5: labeled compound; Merge: overlay) show the results for Control and Fasudil@PDA treatment groups. Scale bar, 10 μm. (**c**) TEM image showing nanoparticle endocytosis. (**d**) TEM image showing nanoparticles in lysosomal compartments (indicated by white arrows). (**e**) Intracellular ROS levels detected by DCFH-DA assay in Bend.3 cells subjected to different treatments: Control (untreated), H_2O_2 (model group), H_2O_2 + Fasudil, H_2O_2 + PDA, and H_2O_2 + Fasudil@PDA. Scale bar, 20 μm. (**f**) Flow cytometry analysis of DCFH-DA fluorescence intensity. (**g**) Quantification of mean DCFH-DA fluorescence intensity by flow cytometry. Data are presented as mean ± SD; ****$p < 0.0001$; ns denotes no significant difference ($p \geq 0.05$).

https://doi.org/10.2147/IJN.S584872

Complementing efficient cellular uptake, Fasudil@PDA significantly alleviated H_2O_2-induced oxidative stress. H_2O_2 treatment markedly elevated ROS levels (~1.5-fold compared to control, $p < 0.0001$). Both Fasudil@PDA and PDA nanoparticles reduced ROS to baseline levels ($p < 0.0001$ vs. H_2O_2 group; Figure 5e–g), whereas free Fasudil showed negligible ROS-scavenging capacity. This confirms that the antioxidant effect is exclusively attributable to the polydopamine (PDA) component.

Together, these findings establish Fasudil@PDA as a promising therapeutic platform for oxidative stress-related vascular disorders. It effectively integrates targeted cellular delivery, inherent antioxidant properties, and intelligent lysosome-activated release mechanisms tailored to the pathological microenvironment.

Fasudil@PDA Nanoparticles Restore Blood-Retinal Barrier Integrity by Targeting the ROCK/MLC Pathway

Diabetic stress triggers RhoA/ROCK signaling, which disrupts the blood-retinal barrier (BRB) primarily through myosin light chain (MLC) phosphorylation-induced actomyosin contraction and tight junction disassembly.[35,36] In bEND.3 cells challenged with advanced glycation end products (AGEs),[37] this pathogenic cascade was evidenced by fragmented ZO-1 immunostaining and a significant downregulation of ZO-1 and occludin proteins (60–70% reduction; $p < 0.01$), concomitant with ROCK1 upregulation (1.8-fold; $p < 0.01$) (Figure 6a–e).

Both free Fasudil and Fasudil@PDA effectively reversed these defects, restoring tight junction protein expression to 65–80% of control levels ($p < 0.01$) via suppression of MLC phosphorylation (Figure 6c–g). Notably, under these controlled in vitro conditions, the two treatments exhibited comparable efficacy, confirming that nano-encapsulation preserves the intrinsic ROCK inhibitory activity of Fasudil. PDA nanoparticles alone showed no significant protective effect.

We next assessed functional recovery in streptozotocin (STZ)-induced diabetic mice. Crucially, in this in vivo setting, Fasudil@PDA demonstrated a definitive advantage, reducing retinal vascular leakage by approximately 50%—significantly outperforming free Fasudil (~30% reduction) and PDA alone (~15%) ($p < 0.0001$; Figure 6h). Retinal flat-mounts visually corroborated that Fasudil@PDA best preserved vascular architecture and minimized FITC-dextran extravasation (Figure 6i–k). This enhanced in vivo efficacy underscores the role of the PDA platform in providing sustained drug release and synergistic antioxidant activity, which collectively mitigate the multifactorial pathology driving vascular hyperpermeability in diabetes.

Anti-Angiogenic Effects of Fasudil@PDA via ROCK/LIMK/Cofilin Pathway Suppression

Beyond vascular leakage, sustained ROCK activation promotes angiogenesis. We investigated whether Fasudil@PDA could inhibit this process by targeting the downstream ROCK/LIMK/cofilin pathway, which regulates actin dynamics and cell migration.[38–40] In AGE-stimulated endothelial cells, Fasudil@PDA treatment suppressed this cascade, reducing ROCK1 expression and phospho-cofilin levels by ~40–50% ($p < 0.01$; Figure 7a–d). This molecular inhibition translated into potent functional effects: cell migration was halved in scratch assays and reduced by 60% in Transwell assays ($p < 0.01$; Figure 7e, f, i and j). Similarly, tube formation under AGE/hypoxia was significantly inhibited by both Fasudil and Fasudil@PDA ($p < 0.01$; Figure 7g, k, l and Figure S10). As with barrier function, the anti-angiogenic efficacy of Fasudil@PDA was equivalent to free Fasudil in vitro. However, in the laser-induced CNV model (which, despite its limitations for DR, is a complex in vivo setting of pathological neovascularization[41,42]), Fasudil@PDA's superior biodistribution and sustained release profile conferred a significant advantage. It reduced CNV area by 45 ± 4.5% ($p < 0.0001$), markedly outperforming free Fasudil (Figure 7h, m and n). Thus, while the core ROCK-inhibiting mechanism is identical, the nanoformulation is critical for delivering this effect optimally to the diseased tissue in vivo.

Fasudil@PDA Alleviates Oxidative Stress and Inflammation via Synergistic Action

Diabetic retinopathy (DR) progression is fueled by a vicious cycle of oxidative stress and chronic inflammation.[43,44] In diabetic retinas, we observed a 3.2-fold increase in oxidative stress and a 2.8-fold rise in activated microglia, alongside elevated pro-inflammatory cytokines (TNF-α, IL-6, IL-1β) (Figure 8a–h).

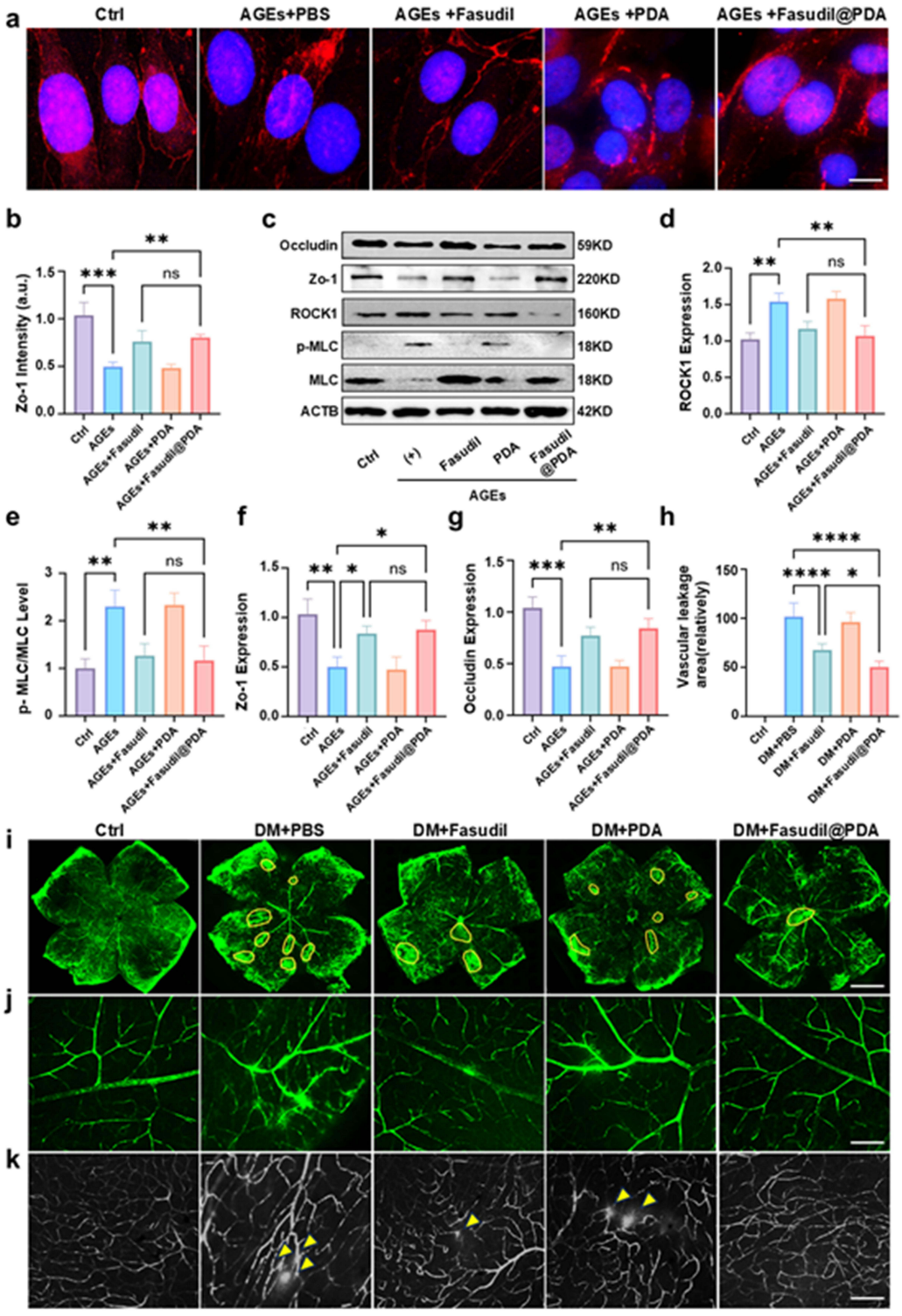

Figure 6 Fasudil@PDA protects vascular integrity through ROCK inhibition and barrier function enhancement. (**a**) ZO-1 immunofluorescence in Bend.3 cells under different treatments: Control, AGEs, AGEs + Fasudil, AGEs + PDA, and AGEs + Fasudil@PDA. (**b**) Quantitative analysis of ZO-1 immunofluorescence intensity. Scale bar, 5 μm. (**c**) Western blot analysis of tight junction and ROCK pathway proteins. (**d** and **e**) Quantitative analysis of ROCK pathway proteins. (**f** and **g**) Quantitative analysis of ZO-1 and Occludin expression. (**h**) Quantitative analysis of vascular leakage assessed by FITC-dextran extravasation in diabetic mice following intravitreal injection of different treatments: Control, DM + PBS, DM + Fasudil, DM + PDA, and DM + Fasudil@PDA. (**i**) Representative fluorescein angiography images of retinal vasculature. Yellow borders indicate the area of vascular leakage visualized by FITC-dextran; Scale bar, 1000 μm. (**j**) High-magnification confocal images of retinal vascular networks. Scale bar, 100 μm. (**k**) Microvascular leakage detection with leakage sites indicated by arrows. Yellow arrows indicate leakage from deep mouse retinal vessels. Scale bar, 100 μm. Data are presented as mean ± SD. *p < 0.05, **p < 0.01, ***p < 0.001, ****p < 0.0001; ns denotes no significant difference (p ≥ 0.05).

https://doi.org/10.2147/IJN.S584872

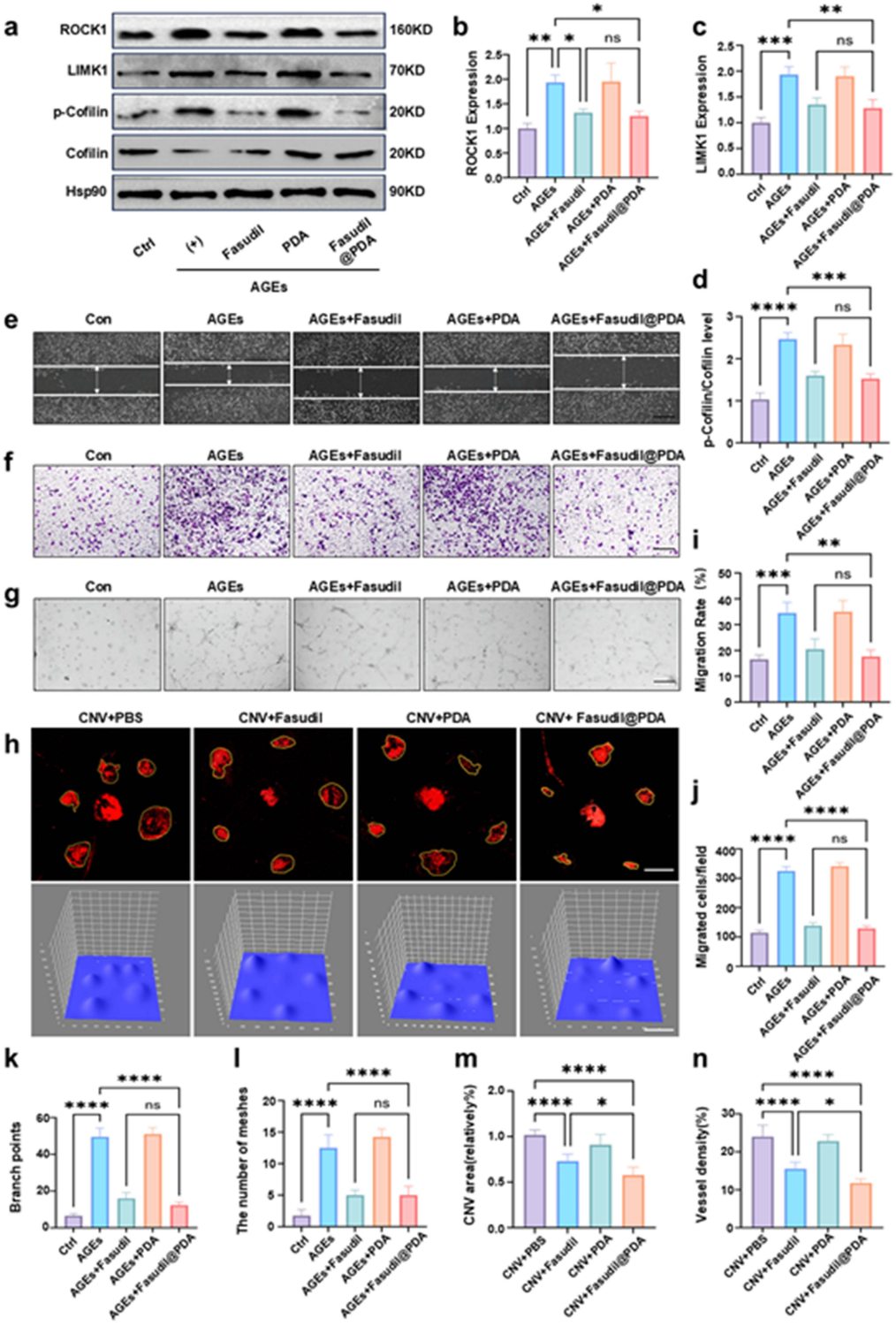

Figure 7 Fasudil@PDA inhibits pathological angiogenesis through ROCK pathway regulation in vitro and in vivo. (**a**) Western blot analysis of ROCK pathway proteins (ROCK1, LIMK1, p-Cofilin, Cofilin, Hsp90) in Bend.3 cells under different treatments: Control, AGEs, AGEs + Fasudil, AGEs + PDA, and AGEs + Fasudil@PDA. (**b** and **c**) Quantification of ROCK1 and LIMK1 levels normalized to Hsp90. (**d**) p-Cofilin/Cofilin ratio. (**e**) Representative images of scratch wound healing assay. Scale bar, 100 μm. (**f**) Representative images of Transwell migration assay. Scale bar, 100 μm. (**g**) Representative images of tube formation assay under AGEs stimulation. Scale bar, 100 μm. (**h**) CD31 immunofluorescence staining of choroidal flat mounts and subsequent quantitative analysis of choroidal neovascularization (CNV) area using ImageJ. Scale bar, 500 μm. (**i**) Quantification of wound closure rate from the scratch assay (**e**). (**j**) Quantification of migrated cell numbers from the Transwell assay (**f**).(**k**) Quantification of branch points from the tube formation assay (**g**), indicating network complexity.(**l**) Quantification of meshes from the tube formation assay (**g**), reflecting network connectivity. (**m**) Quantitative analysis of choroidal neovascularization (CNV) area from CD31-stained flat mounts (**h**). (**n**) Quantitative analysis of vascular density, expressed as the ratio of $CD31^+$ area to total area. Data are presented as mean ± SD; *p < 0.05, **p < 0.01, ***p < 0.001, ****p < 0.0001; ns denotes no significant difference (p ≥ 0.05).

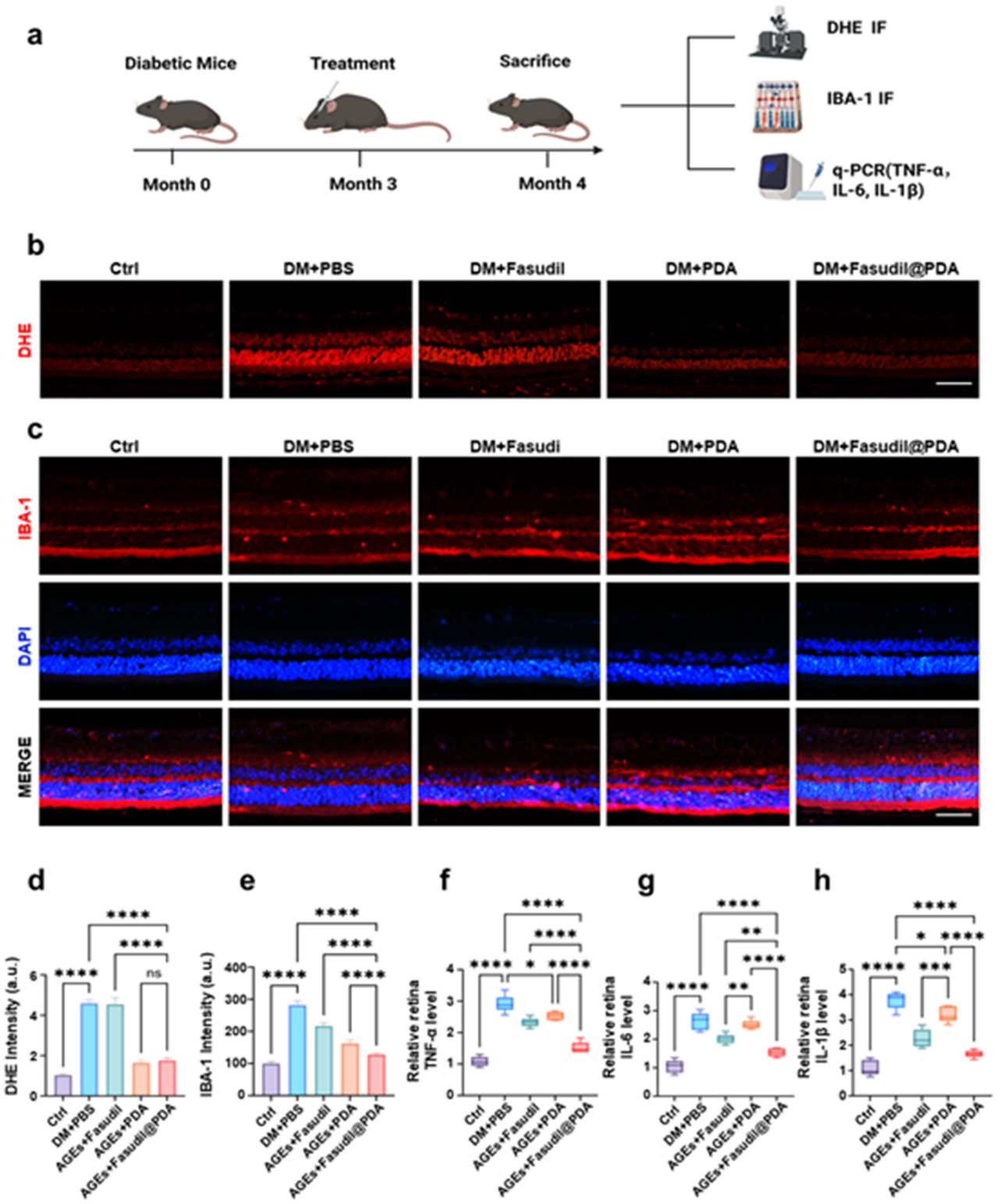

Figure 8 Fasudil@PDA reduces oxidative stress and inflammation in diabetic retina. (**a**) Schematic diagram of the experimental timeline. (**b**) DHE staining of retinal sections. Groups: Ctrl, DM+PBS, DM+Fasudil, DM+PDA, DM+Fasudil@PDA. Scale bar, 50 μm. (**c**) Iba-1 immunofluorescence staining. Scale bar, 50 μm. (**d**) Quantification of DHE fluorescence intensity. (**e**) Quantification of Iba-1$^+$ cells. (**f**) TNF-α mRNA expression level. (**g**) IL-6 mRNA expression level. (**h**) IL-1β mRNA expression level. Data are presented as mean ± SD; *p < 0.05, **p < 0.01, ***p < 0.001, ****p < 0.0001; ns denotes no significant difference (p ≥ 0.05).

https://doi.org/10.2147/IJN.S584872

The key finding was the distinct performance of each treatment. PDA alone modestly attenuated oxidative stress, consistent with its ROS-scavenging property. Free Fasudil also showed partial anti-inflammatory effects.[45,46] Strikingly, Fasudil@PDA consistently and significantly outperformed both individual components ($p < 0.01$), achieving the greatest reduction across all markers of oxidative stress and inflammation. This result demonstrates a true synergistic effect: the PDA carrier not only delivers Fasudil but also concurrently neutralizes the oxidative milieu that fuels inflammation, while Fasudil inhibits ROCK-driven inflammatory signaling. This dual-pathway intervention is uniquely capable of disrupting the self-perpetuating cycle of retinal damage in DR.

Fasudil@PDA Confers Robust Neuroprotection and Preserves Retinal Function

Finally, we evaluated the ultimate therapeutic goal: preserving vision by preventing diabetes-induced neurodegeneration. Diabetic mice exhibited severe functional deficits across retinal layers, indicated by significantly reduced a-wave, b-wave, and oscillatory potential amplitudes ($p < 0.0001$; Figure 9a–c), and a significant loss of retinal ganglion cells (RGCs).

Treatment with Fasudil@PDA led to substantial functional recovery and robustly preserved RGC density (80 ± 5% of non-diabetic levels), effects that were significantly greater than those achieved with free Fasudil or PDA alone ($p < 0.01$; Figure 9d–h). The consistent superiority of the combined nanoformulation underscores that co-targeting oxidative stress (via PDA) and ROCK-dependent inflammatory signaling (via Fasudil) produces synergistic neuroprotection.[47,48] By simultaneously protecting the vasculature and neurons, Fasudil@PDA addresses the multifaceted pathology of DR, positioning it as a comprehensive therapeutic strategy with high clinical translation potential. Nevertheless, the long-term fate of PDA degradation products in the retina is not fully understood, and further investigation into their potential accumulation or inflammatory effects is warranted.

Fasudil@PDA Demonstrates Excellent Local Tolerability and a Favorable Safety Profile

We next evaluated the biosafety of Fasudil@PDA, a critical attribute for clinical translation. In vitro, the nanoparticle showed excellent biocompatibility, causing no significant cytotoxicity in bEnd.3 cells at the therapeutic concentration (40 μg/mL; $p > 0.05$; Figure S11). Free Fasudil and PDA alone were also well tolerated (Figure S12 and S13).

Crucially, in vivo distribution studies confirmed that Cy5-labeled Fasudil@PDA efficiently localized to key retinal layers—particularly the ganglion cell and inner plexiform layers—following intravitreal injection (Figure S14). This targeted engagement underpins its favorable safety profile.[49,50]

Long-term (two-month) intravitreal administration revealed no evidence of local toxicity. Retinal architecture remained intact, with no signs of inflammatory infiltration, degeneration, edema, or atrophy, as confirmed by H&E staining and quantitative thickness analysis (Fasudil@PDA: 225 ± 18 μm vs. PBS: 224 ± 20 μm, $p > 0.05$; Figure S15 and S16).

This compelling safety profile, attributable to the inherent biocompatibility of PDA and the nanoformulation of Fasudil, stands in stark contrast to the systemic side effects (eg., hypotension) that limit the use of conventional ROCK inhibitors.[51,52] By confining high drug exposure to the eye and minimizing systemic diffusion, Fasudil@PDA effectively widens the therapeutic window, solidifying its translational promise for diabetic retinopathy.

Conclusion

In conclusion, we have developed a synergistic nanotherapeutic that simultaneously targets the multiple pathological pathways of diabetic retinopathy (DR). The Fasudil@PDA platform—notable for its straightforward and controllable synthesis without the need for complex modifications—is designed to address the inherent limitations of free Fasudil through enhanced stability and a controlled release profile. Moreover, it combines intrinsic antioxidant activity with microenvironment-responsive release, enabling coordinated mitigation of oxidative stress, vascular leakage, and pathological angiogenesis.

More broadly, this work establishes an innovative paradigm for drug repurposing through rational nanomaterial design. By utilizing pathological cues for spatially and temporally controlled drug activation, we have developed a targeted therapeutic approach that enhances efficacy while reducing systemic side effects. The integration of ROCK

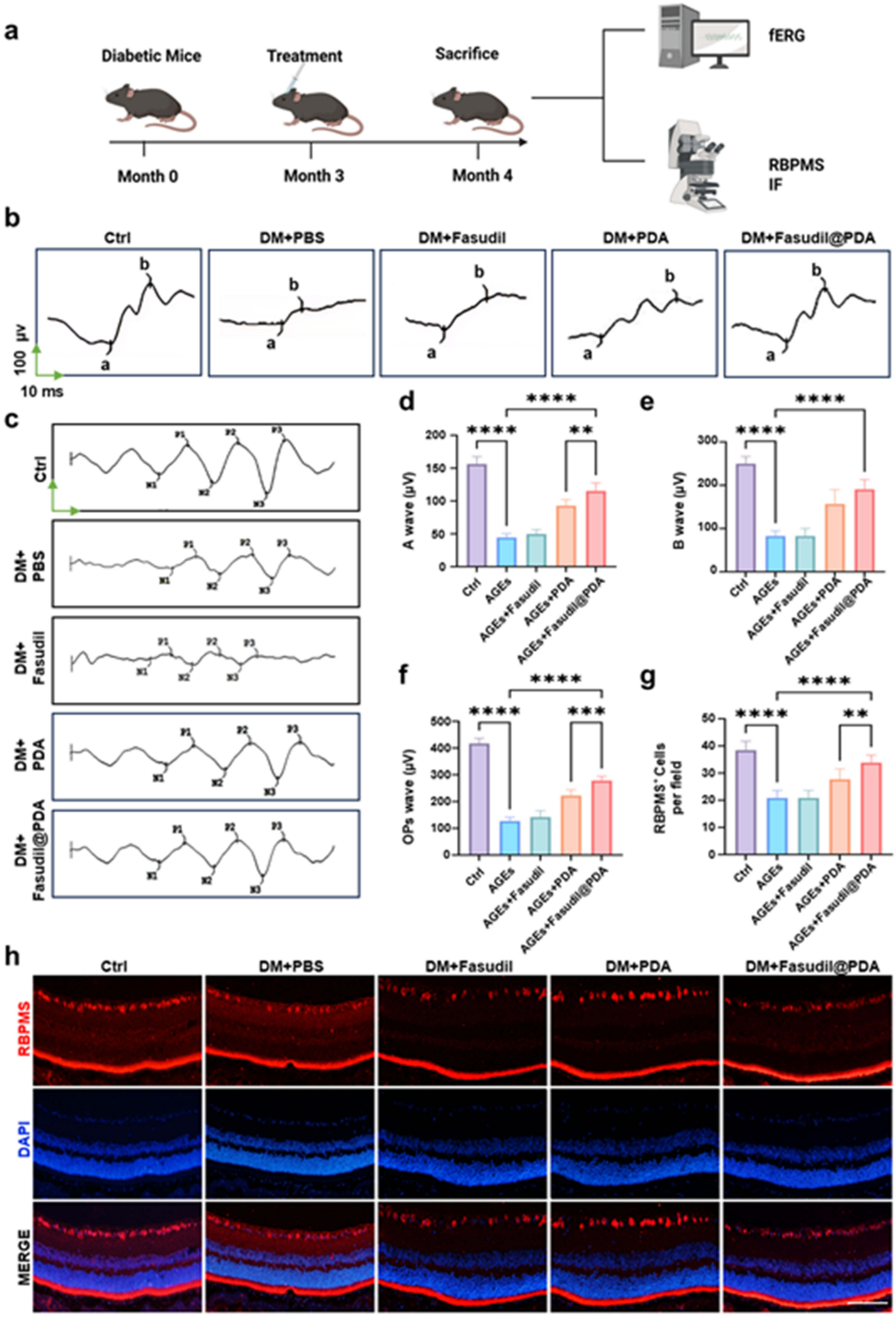

Figure 9 Fasudil@PDA restores retinal function and rescues ganglion cells in diabetic retinopathy. (**a**) Experimental timeline indicating diabetes induction at month 0, treatment initiation at month 3, and final analysis at month 4. (**b**) Representative a-wave and b-wave traces from flash electroretinography (fERG) in Ctrl, DM+PBS, DM +Fasudil, DM+PDA, and DM+Fasudil@PDA groups. The green vertical arrow indicates 100 μV, and the green horizontal arrow indicates 10 ms. (**c**) Representative traces of OPs wave from ERG recordings. The same green arrows as in (**b**) apply. (**d–f**) Quantification of ERG parameters including a-wave amplitude, b-wave amplitude, and OPs wave amplitude. (**g**) Quantification of $RBPMS^+$ retinal ganglion cells across treatment groups. (**h**) Representative immunofluorescence images of RBPMS-labeled retinal ganglion cells; Scale bar, 100 μm. $^{**}p < 0.01$, $^{***}p < 0.001$, $^{****}p < 0.0001$.

https://doi.org/10.2147/IJN.S584872

inhibition with redox modulation in Fasudil@PDA offers a generalizable strategy. This approach could be applicable to other ophthalmologic and inflammatory diseases driven by oxidative stress and signaling dysregulation.

Despite these promising results, we acknowledge certain limitations of our study. The research was conducted primarily in animal models, and further investigations are necessary to validate the clinical applicability and long-term biosafety of this platform in humans. Additionally, the complexity of large-scale nanomedicine manufacturing and sterilization processes warrants further optimization. While the current characterization (DLS, TEM, FTIR, XPS, and release kinetics) is sufficient for the therapeutic conclusions, we recognize that complementary techniques such as solid-state NMR or XRD could provide deeper structural insights in future studies.

Nonetheless, our findings present a compelling candidate for clinical translation in DR and provide a conceptual framework for the development of next-generation nanomedicines capable of intelligent, synergistic, and context-aware therapeutic intervention.

Data Sharing Statement

The datasets generated during the current study are available from the corresponding author upon reasonable request.

Ethics Approval and Consent to Participate

Animal experiments were reviewed and approved by the Animal Care and Use Committee of Huazhong University of Science and Technology (No. TJ-C20230301). All procedures followed the Guide for the Care and Use of Laboratory Animals (8th ed.) and the ARRIVE guidelines.

Acknowledgments

We acknowledge BioRender (BioRender.com) for assistance in creating selected schematics (Fig. 1, 3a, 5a, 8a, and 9a).

Funding

This work was financially supported by grants from the National Natural Science Foundation of China (82472135, 82471103, U24A20707), the National Key Research and Development Program of China (2024YFC2510803), the Natural Science Foundation of Hubei Province (2024AFA053), and the Youth Talent Project of Hubei Provincial Health Commission (WJ2025Q048).

Disclosure

Jiaqi Li, Zheng Zhong and Yin Zhao are co-first authors for this study. The authors declare no competing interests in this work.

References

1. Teo ZL, Whitmarsh W, Virgili G, et al. Global prevalence of diabetic retinopathy and projection of burden through 2045: systematic review and meta-analysis. *Ophthalmology*. 2021;128(11):1580–1591. doi:10.1016/j.ophtha.2021.04.027
2. Antonetti DA, Silva PS, Stitt AW. Current understanding of the molecular and cellular pathology of diabetic retinopathy. *Nat Rev Endocrinol*. 2021;17(4):195–206. doi:10.1038/s41574-020-00451-4
3. Zhou Y, Li J, Zhang L, Wang Y, Yang H, Li X. A glucose-responsive hydrogel inhibits primary and secondary BRB injury for retinal microenvironment remodeling in diabetic retinopathy. *Adv Sci*. 2024;11(32):e2402368. doi:10.1002/advs.202402368
4. Casas AI, Nogales C, Mucke HAM, et al. On the clinical pharmacology of reactive oxygen species. *Pharmacol Rev*. 2020;72(4):801–828. doi:10.1124/pr.120.019422
5. Mateos-Olivares M, Garcia-Onrubia L, Gonzalez-Buendia L, et al. Rho-kinase inhibitors for the treatment of refractory diabetic macular oedema. *Cells*. 2021;10(7):1683. doi:10.3390/cells10071683
6. Xu J, Wang J, Chen X, et al. Acute glucose influx-induced mitochondrial hyperpolarization inactivates myosin phosphatase as a novel mechanism of vascular smooth muscle contraction. *Cell Death Dis*. 2021;12(2):176. doi:10.1038/s41419-021-03462-9
7. Zuo Y, Wang Y, Li J, et al. Controlled delivery of a neurotransmitter-agonist conjugate for functional recovery after severe spinal cord injury. *Nat Nanotechnol*. 2023;18(10):1230–1240. doi:10.1038/s41565-023-01416-0
8. Tan JK, Steel DH, Ahmad S, Viswanathan A, Mathew RG. Exploring the potential of rho kinase inhibitors in ophthalmology: from mechanisms to clinical practice. *Surv Ophthalmol*. 2025;70(5):900–917. doi:10.1016/j.survophthal.2025.03.008
9. Yamaguchi M, Nakayama M, Suzuki Y, et al. Heterotypic macrophages/microglia differentially contribute to retinal ischaemia and neovascularisation. *Diabetologia*. 2024;67(10):2329–2345. doi:10.1007/s00125-024-06215-3

10. Reboussin É, Blouin L, Ghezza S, et al. Evaluation of Rho kinase inhibitor effects on neuroprotection and neuroinflammation in an ex-vivo retinal explant model. *Acta Neuropathol Commun*. 2024;12(1):150. doi:10.1186/s40478-024-01859-z
11. Yuan J, Li S, Wang Y, Zhang H, Chen L, Zhao C. ROCK inhibitor enhances mitochondrial transfer via tunneling nanotubes in retinal pigment epithelium. *Theranostics*. 2024;14(15):5762–5777. doi:10.7150/thno.96508
12. Yao M, Liu R, Li T, et al. CRISPR-CasRx-mediated disruption of Aqp1/Adrb2/Rock1/Rock2 genes reduces intraocular pressure and retinal ganglion cell damage in mice. *Nat Commun*. 2024;15(1):6395. doi:10.1038/s41467-024-50050-4
13. Zhao H, Kong H, Wang W, et al. High glucose aggravates retinal endothelial cell dysfunction by activating the RhoA/ROCK1/pMLC/Connexin43 signaling pathway. *Invest Ophthalmol Vis Sci*. 2022;63(8):22. doi:10.1167/iovs.63.8.22
14. Wang Q, Wang J, Yang XY, Song SS, Han F, Chen HS. Advantages of Rho-associated kinases and their inhibitor fasudil for the treatment of neurodegenerative diseases. *Neural Regen Res*. 2022;17(12):2623–2631. doi:10.4103/1673-5374.335827
15. Stark AK, Penn JS. Prostanoid signaling in retinal cells elicits inflammatory responses relevant to early-stage diabetic retinopathy. *J Neuroinflammation*. 2024;21(1):329. doi:10.1186/s12974-024-03319-w
16. Al-Hilal TA, Park J, Choi JU, Byun Y. Design, synthesis and biological evaluations of a long-acting, hypoxia-activated prodrug of fasudil, a ROCK inhibitor, to reduce its systemic side-effects. *J Control Release*. 2021;334:237–247. doi:10.1016/j.jconrel.2021.04.030
17. Silva M, Matthews Q, Islambulchilar Z, et al. Recent trends in drug-delivery systems for the treatment of diabetic retinopathy and associated fibrosis. *Adv Drug Deliv Rev*. 2021;173:439–460. doi:10.1016/j.addr.2021.04.007
18. Onugwu AL, Nwagwu CS, Onugwu OS, et al. Nanotechnology based drug delivery systems for the treatment of anterior segment eye diseases. *J Control Release*. 2023;354:465–488. doi:10.1016/j.jconrel.2023.01.018
19. Kour J, Kour G, Singh SK, et al. Ocular prodrugs: attributes and challenges. *Asian J Pharm Sci*. 2021;16(2):175–191. doi:10.1016/j.ajps.2020.08.002
20. Wolff AW, Gensler S, Schreglmann SR, et al. SAFE-ROCK: a Phase I Trial of an Oral Application of the ROCK Inhibitor Fasudil to Assess Bioavailability, Safety, and Tolerability in Healthy Participants. *CNS Drugs*. 2024;38(4):291–302. doi:10.1007/s40263-024-01070-7
21. Zhang Y, Wang C, Li Z, Liu Y, Zhang X. Intravitreal therapeutic nanoparticles for age-related macular degeneration: design principles, progress and opportunities. *Adv Colloid Interface Sci*. 2024;329:103200. doi:10.1016/j.cis.2024.103200
22. Lou X, Zhang Y, Li W, et al. Polydopamine nanoparticles attenuate retina ganglion cell degeneration and restore visual function after optic nerve injury. *J Nanobiotechnology*. 2021;19(1):436. doi:10.1186/s12951-021-01199-3
23. He L, Wang Y, Zhao C, Zhang X, Liu Y, Chen J. Multifunctional dynamic chitosan-guar gum nanocomposite hydrogels in infection and diabetic wound healing. *Carbohydr Polym*. 2025;354:123316. doi:10.1016/j.carbpol.2025.123316
24. Jiang D, Liu Y, Wang J, Feng Z, Li H, Zhang Q. Broad-spectrum downregulation of inflammatory cytokines by polydopamine nanoparticles to protect the injured spinal cord. *Acta Biomater*. 2025;193:559–570. doi:10.1016/j.actbio.2024.12.028
25. Zhou Z, Zhou C, Liu J, Yuan Y, Yao C, Liu M. Tumor specific in situ synthesis of therapeutic agent for precision cancer therapy. *J Nanobiotechnology*. 2024;22(1):612. doi:10.1186/s12951-024-02825-6
26. Ding Y, Sun C, Wang Z, Li Y, Zhang X, Wang J. Lipid prodrug nanoassemblies via dynamic covalent boronates. *ACS Nano*. 2023;17(7):6601–6614.
27. Han X, Zhang L, Kong L, et al. Comprehensive metabolic profiling of diabetic retinopathy. *Exp Eye Res*. 2023;233:109538. doi:10.1016/j.exer.2023.109538
28. Pandit J, Sultana Y, Aqil M. Chitosan coated nanoparticles for efficient delivery of bevacizumab in the posterior ocular tissues via subconjunctival administration. *Carbohydr Polym*. 2021;267:118217. doi:10.1016/j.carbpol.2021.118217
29. Lei T, Zhang X, Du H, et al. A nanocleaner specifically penetrates the blood–brain barrier at lesions to clean toxic proteins and regulate inflammation in Alzheimer's disease. *Acta Pharm Sin B*. 2021;11(12):4032–4044. doi:10.1016/j.apsb.2021.04.022
30. Mietzner R, Stork L, Storp JJ, et al. Fasudil loaded PLGA microspheres as potential intravitreal depot formulation for glaucoma therapy. *Pharmaceutics*. 2020;12(8):706. doi:10.3390/pharmaceutics12080706
31. Kang Q, Yang C. Oxidative stress and diabetic retinopathy: molecular mechanisms, pathogenetic role and therapeutic implications. *Redox Biol*. 2020;37:101799. doi:10.1016/j.redox.2020.101799
32. Gui SY, Wang YF, Li J, et al. Nanoscale coordination polymer Fe-DMY downregulating Poldip2-Nox4-H2O2 pathway and alleviating diabetic retinopathy. *J Pharm Anal*. 2023;13(11):1326–1345. doi:10.1016/j.jpha.2023.05.002
33. Cheng X, Li D, Sun M, Wang J, Liu Y, Zhang X. Self-assembled ternary hybrid nanodrugs for overcoming tumor resistance and metastasis. *Acta Pharm Sin B*. 2021;11(11):3595–3607. doi:10.1016/j.apsb.2021.03.041
34. Nguyen DD, Chia SS, Venkatraman SS, Agrawal R, Wong TT. Highly retina-permeating and long-acting resveratrol/metformin nanotherapeutics for enhanced treatment of macular degeneration. *ACS Nano*. 2023;17(1):168–183. doi:10.1021/acsnano.2c05824
35. Sasaki J, Matsuoka Y, Kawasaki R, Tsubota K, Ozawa Y. Relevance of diabetic retinopathy with AGEs and carotenoid levels assessed by skin sensors. *Antioxidants*. 2022;11(7):1370. doi:10.3390/antiox11071370
36. Zhou W, Li H, Wang J, Zhang Y, Liu Y. Retinol binding protein 4 promotes the phenotypic transformation of vascular smooth muscle cells under high glucose condition via modulating RhoA/ROCK1 pathway. *Transl Res*. 2023;259:13–27. doi:10.1016/j.trsl.2023.03.004
37. Dorweiler TF, Torretti B, Prusakov AG, et al. Diabetic retinopathy is a ceramidopathy reversible by anti-ceramide immunotherapy. *Cell Metab*. 2024;36(7):1521–33.e5. doi:10.1016/j.cmet.2024.04.013
38. Nagai Y, Matoba K, Kawanami D, et al. Rho-associated, coiled-coil-containing protein kinase 1 regulates development of diabetic kidney disease via modulation of fatty acid metabolism. *Kidney Int*. 2022;102(3):536–545. doi:10.1016/j.kint.2022.04.021
39. Balafouti S, Penning LC, Kotsantis P, et al. Tension-sensitive LINC-RhoA signaling prevents chromatin bridge breakage in cytokinesis. *EMBO J*. 2025;44(18):e113452. doi:10.1038/s44318-025-00565-3
40. Noh JM, Kim JH, Lee SJ, et al. The activation of the LIMK/Cofilin signaling pathway via extracellular matrix-integrin interactions is critical for the generation of mature and vascularized cardiac organoids. *Cells*. 2023;12(16):2029. doi:10.3390/cells12162029
41. Ni B, Li T, Wang J, et al. Therapeutic intervention in neuroinflammation for neovascular ocular diseases through targeting the cGAS-STING-necroptosis pathway. *J Neuroinflammation*. 2024;21(1):164. doi:10.1186/s12974-024-03155-y
42. Ang KH, Wang Y, Li J, et al. PRL3-zumab as an anti-angiogenic therapy in neovascular eye diseases. *Nat Commun*. 2025;16(1):4791. doi:10.1038/s41467-025-59929-2

43. Church KA, Silverman SM, Wong WT. Pharmacological depletion of microglia alleviates neuronal and vascular damage in the diabetic CX3CR1-WT retina but not in CX3CR1-KO or hCX3CR1I249/M280-expressing retina. *Front Immunol*. 2023;14:1130735. doi:10.3389/fimmu.2023.1130735
44. Zhu J, Wang Y, Li X, Chen Z, Liu Y. Emerging role of extracellular vesicles in diabetic retinopathy. *Theranostics*. 2024;14(4):1631–1646. doi:10.7150/thno.92463
45. Huyan T, Li Q, Wang Y, Zhang L, Chen Z, Liu Y. ROCK1 inhibition improves wound healing in diabetes via RIPK4/AMPK pathway. *Acta Pharmacol Sin*. 2024;45(7):1477–1491. doi:10.1038/s41401-024-01246-3
46. Tang L, Xu X, Zhang Y, Wang Y, Li X. Inflammation in diabetic retinopathy: possible roles in pathogenesis and potential implications for therapy. *Neural Regen Res*. 2023;18(5):976–982. doi:10.4103/1673-5374.355743
47. Kowluru RA, Mishra M. Oxidative stress, mitochondrial damage and diabetic retinopathy. *Biochim Biophys Acta*. 2015;1852(11):2474–2483. doi:10.1016/j.bbadis.2015.08.001
48. Wang J, Chen C, Li S, et al. Rho-associated kinase inhibitor suppresses oxidative stress-induced vascular endothelial growth factor production in diabetic retinopathy. *J Pharmacol Exp Ther*. 2016;359(1):45–53. doi:10.1124/jpet.116.235069
49. Sun D, Zhou S, Gao W. What went wrong with anticancer nanomedicine design and how to make it right. *ACS Nano*. 2020;14(10):12281–12290. doi:10.1021/acsnano.9b09713
50. Song R, Wang J, Li Y, Zhang X, Liu Y, Chen Z. Optimizing surface maleimide/cRGD ratios enhances targeting efficiency of cRGD-functionalized nanomedicines. *J Am Chem Soc*. 2025;147(3):2889–2901. doi:10.1021/jacs.4c17178
51. Shimokawa H, Takeshita A. Long-term inhibition of Rho-kinase induces a regression of arteriosclerotic lesions and enhances eNOS expression in spontaneously hypertensive rats. *J Cardiovasc Pharmacol*. 2003;41(1):S1–6.
52. Honjo M, Tanihara H. Impact of the clinical use of ROCK inhibitor on the pathogenesis and treatment of glaucoma. *Jpn J Ophthalmol*. 2018;62(2):109–126. doi:10.1007/s10384-018-0566-9